

Multi-Frequency Observations of the Candidate Neutrino Emitting Blazar BZB J0955+3551

VAIDEHI S. PALIYA,¹ M. BÖTTCHER,² A. OLMO-GARCÍA,³ A. DOMÍNGUEZ,⁴ A. GIL DE PAZ,⁴ A. FRANCKOWIAK,¹
S. GARRAPPA,¹ AND R. STEIN¹

¹*Deutsches Elektronen Synchrotron DESY, Platanenallee 6, 15738 Zeuthen, Germany*

²*Centre for Space Research, North-West University, Potchefstroom, 2531, South Africa*

³*Universidad Complutense de Madrid (UCM, Spain) and Instituto de Física de Partículas y del Cosmos (IPARCOS)*

⁴*IPARCOS and Department of EMFTEL, Universidad Complutense de Madrid, E-28040 Madrid, Spain*

Submitted to ApJ

ABSTRACT

The recent spatial and temporal coincidence of the blazar TXS 0506+056 with the IceCube detected neutrino event IC-170922A, has opened up a realm of multi-messenger astronomy with blazar jets as a plausible site of cosmic-ray acceleration. After TXS 0506+056, for the first time, a second blazar, BZB J0955+3551, has recently been found to be spatially coincident with the IceCube detected neutrino event IC-200107A and undergoing its brightest X-ray flare measured so far. Here, we present the results of our multi-frequency campaign to study this peculiar event that includes observations with the *NuSTAR*, *Swift*, *NICER*, and 10.4 m Gran Telescopio Canarias (GTC). The optical spectroscopic observation from GTC secured its redshift as $z = 0.5573$. Both *NuSTAR* and *NICER* data reveal a rapid flux variability albeit at low-significance ($\lesssim 3.5\sigma$). We explore the origin of the target photon field needed for the photo-pion production using analytical calculations and considering the observed optical-to-X-ray flux level and conclude that seed photons must come from outside the jet, similar to that reported for TXS 0506+056. We find that there could be a sub-dominant hadronic population responsible for the neutrino emission.

Keywords: galaxies, active — galaxies: Evolution — galaxies: interactions — galaxies: jets

1. INTRODUCTION

High-energy neutrinos are unique messengers originating from the extreme physical processes in the Universe. Being solely produced in hadronic interactions of high-energy cosmic-ray nuclei with ambient matter or photon fields, they provide the smoking gun signature for hadronic acceleration sites.

Blazars, i.e., radio-loud quasars with powerful relativistic jets aligned to our line of sight, have been suggested as potential cosmic-ray and neutrino sources (see, e.g., Mannheim et al. 1992; Petropoulou et al. 2015; Murase 2017; Lucarelli et al. 2019; Garrappa et al. 2019; Giommi et al. 2020a). The most compelling high-energy neutrino source candidate identified so far is the blazar TXS 0506+056 (IceCube Collaboration et al. 2018a,b).

The 290 TeV neutrino IC-170922A was found in spatial coincidence with TXS 0506+056 and arrived during a major outburst observable in all wavelengths (IceCube Collaboration et al. 2018a). Interestingly an archival search for lower-energy $\mathcal{O}(10\text{ TeV})$ neutrinos revealed a neutrino flare in 2014/15, which lasted 160 days, but was not accompanied by activity in the electromagnetic regime (IceCube Collaboration et al. 2018b). From a theoretical perspective, Reimer et al. (2019) proposed that there should not be a strongly correlated gamma-ray and neutrino activity, and that neutrino production activity (through associated cascading) might actually show up more clearly in X-rays.

BL Lacertae objects (or BL Lacs) are a sub-population of blazars that exhibits an optical spectrum lacking any emission lines with equivalent width $> 5\text{ \AA}$ (e.g., Stickel et al. 1991). Their optical spectra are power-law dominated indicating either especially strong non-thermal continuum (due to Doppler boosting) or unusually weak thermal disk/broad line emission (plausibly attributed

to low accretion activity; [Giommi et al. 2012](#)). BL Lacs that have the synchrotron peak located at very high frequencies ($\nu_{syn}^{peak} > 10^{17}$ Hz) are termed as extreme blazars (e.g., [Costamante et al. 2001](#); [Foffano et al. 2019](#); [Paliya et al. 2019](#)). The observation of such a high synchrotron peak frequency indicates them to host some of the most efficient particle accelerator jets. Interestingly, extreme blazars are also proposed as promising candidates of high-energy neutrinos (cf. [Petropoulou et al. 2015](#); [Padovani et al. 2016](#)).

So far, any clustering of neutrinos in either space or time have not been confirmed in the all-sky searches of IceCube data ([Aartsen et al. 2015, 2017](#); [Aartsen et al. 2020](#)). Therefore, a promising methodology could be the search for transient and variable electromagnetic sources temporally and spatially coincident with IceCube neutrino events using multi-frequency observations.

In this regard, the identification of a γ -ray detected extreme blazar, BZB J0955+3551 (also known as 4FGL J0955.1+3551), found both in temporal (in X-rays) and spatial coincidence with the IceCube detected neutrino event IC-200107A ([IceCube Collaboration 2020](#); [Giommi et al. 2020b](#); [Krauss et al. 2020](#)) has provided an interesting case for blazar jets as a plausible source of cosmic neutrinos. In fact, a prompt *Swift*-XRT target of opportunity (ToO) observation of BZB J0955+3551 on 2020 January 8 found it to be undergoing its brightest X-ray flare measured so far. Another γ -ray detected blazar, 4FGL J0957.8+3423, was found to lie within the 90% positional uncertainty of IC-200107A, however, no significant flux enhancement was noticed from this object in X- or γ -rays ([Krauss et al. 2020](#); [Garrappa et al. 2020](#)).

Motivated by the identification of a candidate neutrino emitting blazar undergoing an X-ray outburst close in time to the neutrino arrival, we started a multi-wavelength campaign. This includes a Director’s Discretionary Time (DDT) observation with the Nuclear Spectroscopic Telescope Array (*NuSTAR*) and multiple *Swift* target of opportunity (ToO) observations. An optical spectroscopic followup with 10.4 m Gran Telescopio Canarias (GTC) was carried out to determine the spectroscopic redshift of BZB J0955+3551. In addition to that, the source was also observed with the Neutron star Interior Composition Explorer (*NICER*) simultaneous to the *NuSTAR* pointing as a part of DDT ToO invoked by the mission principal investigator. Here, we present the results of the conducted multi-frequency campaign along with theoretical interpretation of the event with the primary objective to explore the broad-band flaring behavior of the source and physical processes that may explain the IceCube detected neutrino.

In Section 2, we describe the steps adopted to analyze various data sets. Results are presented in Section 3 and discussed in Section 4. We summarize our findings in Section 5. Throughout, we adopt a Cosmology of $H_0 = 67.8 \text{ km s}^{-1} \text{ Mpc}^{-1}$, $\Omega_m = 0.308$, and $\Omega_\Lambda = 0.692$ ([Planck Collaboration et al. 2016](#)).

2. DATA REDUCTION AND ANALYSIS

2.1. Optical Spectroscopy with GTC

In order to determine the redshift of the source BZB J0955+3551, we took optical spectra with the instrument OSIRIS ([Cepa et al. 2000, 2003](#)) at the GTC telescope. The 0.8 arcsec-wide slit was positioned to cover the source and a companion ~ 3 arcsec south-east to the blazar (see Figure 1). The total integration time was ~ 2 hrs divided into 6 exposures of 1098 s each. The chosen grism was R1000R, which covers the spectral range of 5100 - 10000 Å with a resolution of 1122¹. This grism was selected due to its large spectral range and good spectral resolution, which provides a large pool to find emission or absorption lines and calculate the redshift of the source.

The raw data was reduced using the standard procedure with the IRAF tasks, through the PyRAF software². The main steps are: bias and flat correction, cosmic-ray removal, wavelength calibration, sky subtraction, spectra extraction and flux calibration. The cosmic rays were removed in each individual science spectrum with the IRAF task `lacos_spec` ([van Dokkum 2001](#)). The wavelength calibration was done with a combination of arcs from three different lamps (HgAr, Ne and Xe) to cover all the wavelength range of the spectra. The sky was subtracted with the IRAF task `background`, selecting background samples to the right of the blazar and to the left on the companion, and fitted with a Chebyshev polynomial of order 3. After this step, the science spectra were combined, which removed any cosmic-ray residual. The spectrum of the blazar and the companion were extracted independently from the combined science spectra. The extraction was done with the IRAF task `apall`, optimising the apertures to extract the most flux from the sources. For the flux calibration, the spectrophotometric standard star G191-B2B was observed on the same night of the observation. This calibration included atmospheric extinction correction at the observatory ([King 1985](#)). Each spectrum was flux calibrated to convert from counts to absolute

¹ <http://www.gtc.iac.es/instruments/osiris/osiris.php>

² PyRAF is a product of the Space Telescope Science Institute, which is operated by AURA for NASA http://www.stsci.edu/institute/software_hardware/pyraf/

flux units, and corrected from Galactic extinction using the IRAF task `deredden` with the values $R = 3.1$, $E(B - V) = 0.0109$ (Schlafly & Finkbeiner 2011).

2.2. *NuSTAR*, *NICER*, and *Swift*

NuSTAR observed BZB J0955+3551 on 2020 January 11 for a net exposure of 25.6 ksec under our DDT request (observation id: 90501658002). We first cleaned and calibrated the event file using the tool `nupipeline`. We define the source and background regions as circles of $30''$ and $70''$, respectively. The former was centered at the target blazar and the latter from a nearby region on the same chip and avoiding source contamination. The pipeline `nuproducts` was used to extract light curves, spectra, and ancillary response files. In the energy range of 3–79 keV, a binning of 1.5 ksec was adopted to generate the light curve and the source spectrum was binned to have at least 20 counts per bin.

NICER observed BZB J0955+3551 for a net exposure of ~ 11 ksec, simultaneous to the *NuSTAR* pointing on 2020 January 11 as a DDT target of opportunity (ToO observation id: 2200990102). We analyzed the *NICER* data with the latest software HEASOFT 6.26.1 and calibration files (v. 20190516). In particular, the pipeline `nicer12` was adopted with default settings to select all 56 detectors, apply standard filters and calibration to clean the events and finally merge them to generate one event file. We then used the tool `xselect` to extract the source spectrum and 3 minutes binned light curve. The background was estimated using the tool `nicer_bkg_estimator`³ (K. Gendreau et al. in preparation). The quasar spectrum was binned to 20 counts per bin.

Contemporaneous to the arrival of IC-200107A neutrino, ToO observations of BZB J0955+3551 from the *Swift* satellite were carried out on 2020 January 8 (Giommi et al. 2020b; Krauss et al. 2020) and 11. We first cleaned and calibrated the X-ray Telescope (XRT) data taken in the photon counting mode with the tool `xrtpipeline` and by adopting the latest CALDB (v. 20200106). Exposure maps and ancillary response files were generated with the tasks `ximage` and `xrtmkarf`, respectively. To extract the source spectrum, we considered a circular region of $47''$, which encloses about 90% of the XRT point spread function, centered at the target. The background was estimated from an annular region centered at the target with inner and outer radii $70''$ and $150''$, respectively. We binned the blazar spectrum to 20 counts per bin.

The X-ray spectral analysis was carried out in XSPEC (Arnaud 1996) and the Galactic neutral hydrogen column density ($N_{\text{H}} = 1.14 \times 10^{20} \text{ cm}^{-2}$) was adopted from Kalberla et al. (2005). The XRT spectrum taken on January 8 is well explained with a simple absorbed power-law model. On the other hand, joint *NICER* and *NuSTAR* spectra from January 11, are better fitted with an absorbed log parabola model, clearly revealing the synchrotron peak.

Individual snapshots taken from the *Swift* UltraViolet Optical Telescope (UVOT) were first combined using the pipeline `uvotimsum` and then photometry was performed with the task `uvotsource`. For the latter, we considered a source region of $2''$, avoiding the nearby object located $\sim 3''$ South-East of BZB J0955+3551. The background is estimated from a $30''$ circular region free from the source contamination. The derived magnitudes were corrected for Galactic extinction (Schlafly & Finkbeiner 2011) and converted to flux units following zero points adopted from Breeveld et al. (2011).

2.3. Others

BZB J0955+3551 remained below the detection threshold of the *Fermi*-Large Area Telescope at the time of the neutrino arrival (Garrappa et al. 2020). Therefore, we used the spectral parameters provided in the recently released fourth catalog of the *Fermi*-LAT detected objects (4FGL; The *Fermi*-LAT collaboration 2019) to get an idea about the average γ -ray behavior of the source. In addition to that, we used archival measurements from the Space Science Data Center⁴. These are not used for the modeling, however, can provide a meaningful information about the typical activity state of the source.

3. RESULTS

The i' filter image of BZB J0955+3551 taken with the Panoramic Survey Telescope and Rapid Response System (Pan-STARRS) is shown in Figure 1. A faint companion object (i' magnitude = 20.85 ± 0.36) located $\sim 3''$ South-East of the blazar (i' magnitude = 19.17 ± 0.06) can be seen. Since both objects lacked spectroscopic redshift information, we carried out a long-slit spectroscopy of the system with OSIRIS mounted at GTC. The resultant optical spectra are shown in Figure 1.

Various absorption lines associated with the host galaxy, e.g., Ca II H&K doublet, are identified in the optical spectrum of the blazar. Additionally, we also detected a weak [O II]3727 emission line with rest-frame equivalent width of $0.15 \pm 0.05 \text{ \AA}$. These allowed

³ https://heasarc.gsfc.nasa.gov/docs/nicer/tools/nicer_bkg_est_tools.html⁴ <https://tools.ssdsc.asi.it/>

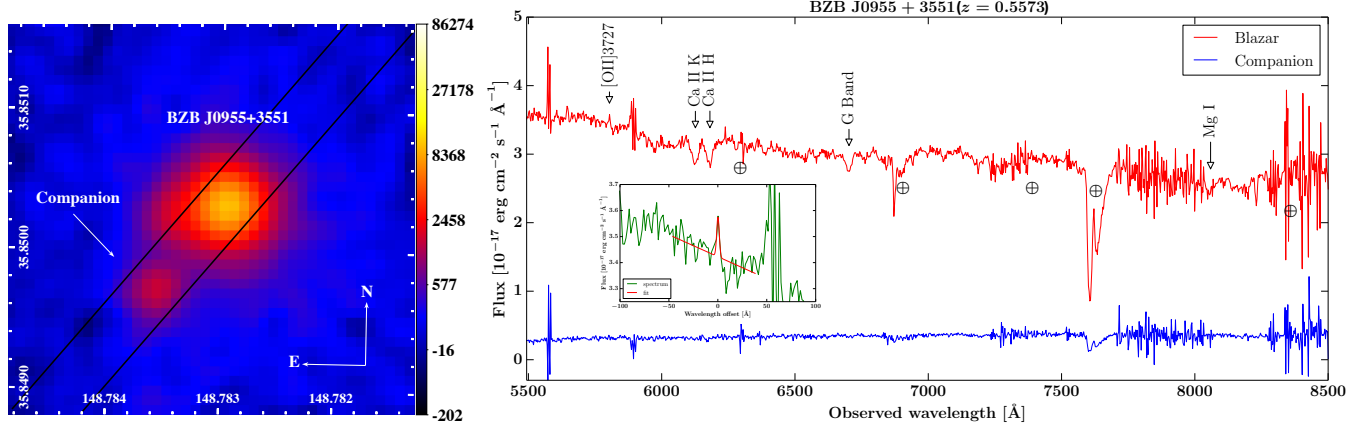


Figure 1. Left: Pan-STARRS i' filter image of BZB J0955+3551. Note the presence of a faint companion object at $\sim 3''$ South-East of the blazar. Parallel black lines represent the slit position for the long-slit spectrograph OSIRIS. The colorbar represents the Pan-STARRS count units. Right: Optical spectra of the source BZB J0955+3551 and the companion taken at GTC with OSIRIS. The red line is the spectrum of the blazar and the blue line is the spectrum of the companion. The identified emission and absorption lines are marked with vertical arrows and labeled correspondingly. The atmospheric absorption features are marked with the symbol \oplus . The inset shows the fit of the emission line [OII]3727 to derive its luminosity and equivalent width. The spectrum is shown in a green line and the fit in a red line. The continuum is fit with a power-law and the line with a single Gaussian function. The wavelength of the line has been subtracted from the x-axis.

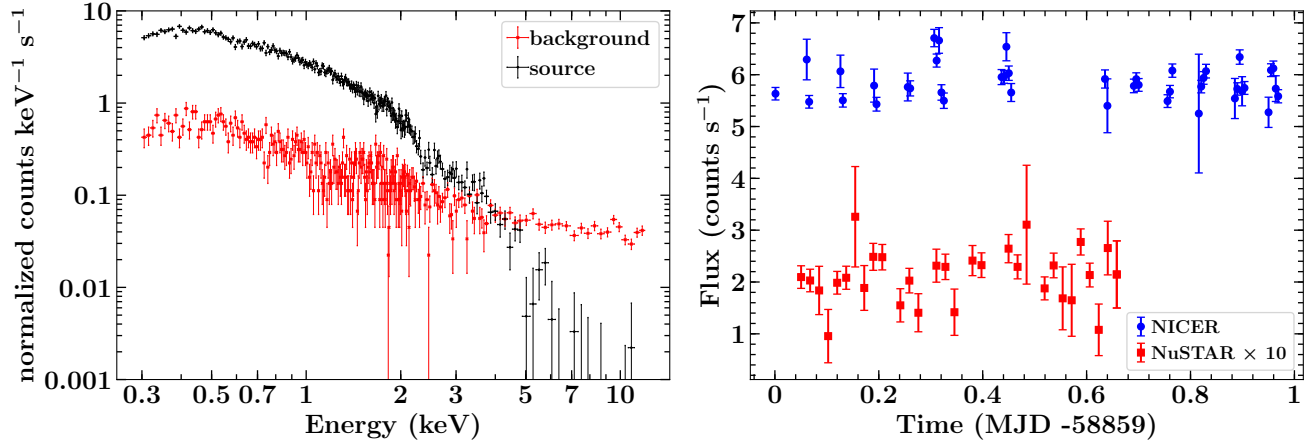


Figure 2. Left: The count spectra of BZB J0955+3551 (black) and the background (red). As can be seen, at $\gtrsim 5$ keV, the background dominates the observed counts. Right: 1.5 ksec binned *NuSTAR* (3–79 keV) and 3 minutes binned *NICER* (0.3–5 keV) light curves of BZB J0955+3551. The flux of the former is multiplied by 10 for a meaningful comparison.

us to firmly establish the redshift of BZB J0955+3551 as $z = 0.5573$. The spectrum of the companion does not reveal any noticeable feature. Deeper spectroscopic observations are necessary to characterize this object and to explore the possibility of its interaction/merger with BZB J0955+3551.

In order to ascertain the impact of the background on the *NICER* observation, we plot the count spectrum of the source and background in Figure 2. As can be seen, the *NICER* spectrum remains source dominated up to ~ 5 keV (see Figure 2, left panel). Therefore, we used 0.3–5 keV energy range to extract the *NICER* light curve and spectrum of BZB J0955+3551.

In Figure 2, we show the *NICER* and the *NuSTAR* light curves. The light curves are scanned to search for rapid flux variations. This was done by computing the flux doubling/halving time (τ) as follows:

$$F(t_2) = F(t_1) \cdot 2^{(t_2 - t_1)/\tau} \quad (1)$$

where $F(t_1)$ and $F(t_2)$ are the fluxes at time t_1 and t_2 respectively. The uncertainties in the flux values were taken into account by setting the conditions that the difference in fluxes at the epochs t_1 and t_2 is at least 2σ significant.

We found evidence of rapid flux variations in the *NICER* data with the shortest flux halving time of

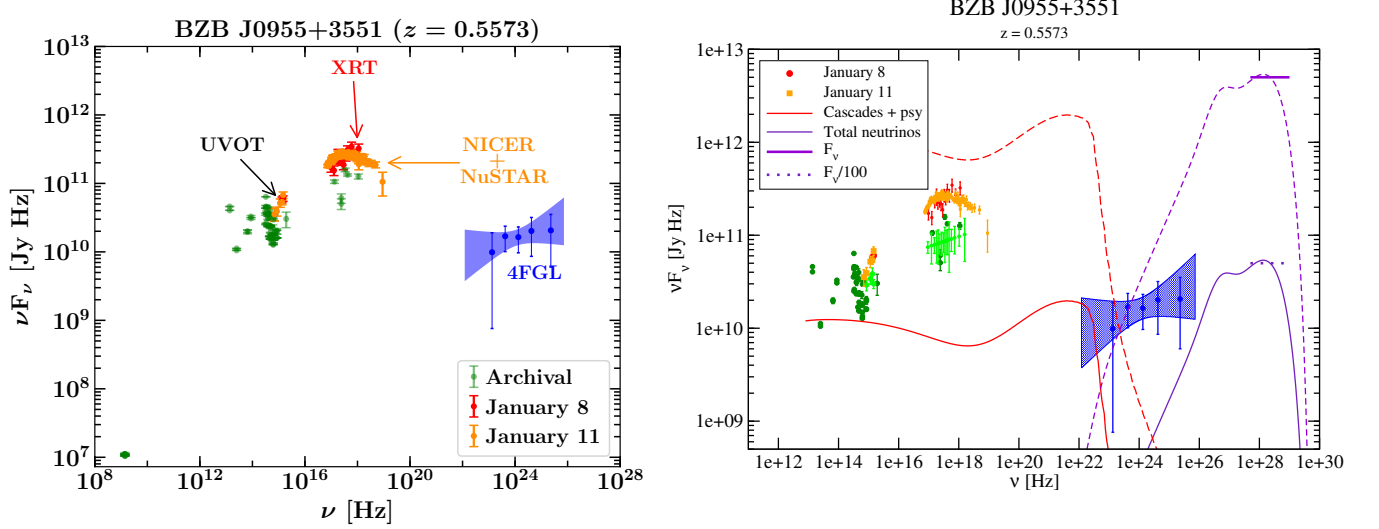


Figure 3. Left: Broadband SED of BZB J0955+3551 generated using the data acquired on January 8 (red) and 11 (yellow) and also considering archival observations (green). In the *Fermi*-LAT energy range, we show the bow-tie and spectral data points adopted from the 4FGL catalog. Right: Same as left but also plotting the results of the hadronic simulation performed using the parameters constrained from the observed optical-to-X-ray spectrum and derived from the analytical calculations in Section 4.2. We divide the expected neutrino flux of 5×10^{-11} erg cm $^{-2}$ s $^{-1}$ (violet solid horizontal line) by a factor of 100 (violet dotted horizontal line) to take into account the Eddington bias (cf. [Strotjohann et al. 2019](#)).

Table 1. Summary of the SED analysis.

Epoch	Γ_X/α	β	X-ray		
			Normalization	Statistics	Instrument
January 8	$1.74^{+0.11}_{-0.10}$	—	$14.11^{+1.03}_{-1.03}$	22.93/27	<i>Swift</i> -XRT
January 11	$2.13^{+0.04}_{-0.04}$	$0.17^{+0.04}_{-0.03}$	$1.74^{+0.08}_{-0.07}$	456.94/462	<i>NICER</i> + <i>NuSTAR</i>
<i>Swift</i> -UVOT					
Epoch	B	U	$UVW1$	$UVM2$	$UVW2$
January 8	—	—	—	5.75 ± 0.56	6.03 ± 0.54
January 11	3.54 ± 0.72	3.91 ± 0.58	5.20 ± 0.72	5.36 ± 0.51	6.75 ± 0.74

NOTE—*Swift*-XRT spectral fitting (January 8) is done in the energy range of 0.3–10 keV, whereas, it is 0.3–79 keV for the joint *NICER* and *NuSTAR* analysis (January 11). Γ_X is the power-law X-ray photon index and α and β are the log-parabolic photon index at the pivot energy (fixed at 1 keV) and curvature around the peak, respectively. The X-ray normalization has the unit of 10^{-4} ph cm $^{-2}$ s $^{-1}$ keV $^{-1}$. The flux values reported for the five *Swift*-UVOT filters are in 10^{-13} erg cm $^{-2}$ s $^{-1}$.

28.3 ± 7.9 minutes at 3.5σ significance level. The *NuSTAR* light curve also revealed traces of fast variability with the shortest flux doubling time of 19.2 ± 10.7 minutes, albeit at a low 2.2σ confidence level.

The broadband spectral energy distribution (SED) of BZB J0955+3551 during the January 8 and 11 epochs is shown in Figure 3. The archival IR-optical spectrum reveals a bump which is likely to be originated from the host galaxy and has been noticed in many extreme blazars (see, e.g., [Costamante et al. 2018](#)). The long-time averaged 4FGL SED reveals an extremely hard γ -ray spectrum suggesting the inverse Compton peak to be located at very high energies (>100 GeV). Note that

at this redshift the extragalactic background light attenuation is also significant ([Domínguez et al. 2011](#)).

4. DISCUSSION

4.1. Properties of the Central Engine

We have derived the central black hole mass (M_{BH}) of BZB J0955+3551 using its r' band magnitude and considering the host galaxy to be a giant elliptical. The known empirical relation between the absolute magnitude ($M(R)$) of the bulge and M_{BH} was adopted following [McLure & Dunlop \(2002\)](#). The estimated M_{BH} is $6.4 \times 10^8 M_{\odot}$ with a typical uncertainty of ~ 0.4 dex ([McLure & Dunlop 2002](#)).

Furthermore, we computed the [OII]3727 line luminosity as $\sim 6 \times 10^{39} \text{ erg s}^{-1}$ by fitting the continuum around the emission line in the OSIRIS spectrum with a power-law and the emission line with a Gaussian function (see inset in Figure 1). From the derived line luminosity, we estimated the bolometric luminosity as $1 \times 10^{45} \text{ erg s}^{-1}$, after correcting for the possible jet contamination (see Punsly & Zhang 2011; Padovani et al. 2019). Assuming the accretion disk luminosity (L_{disk}) to be half of the bolometric one (e.g., Richards et al. 2006), we get $L_{\text{disk}} = 5 \times 10^{44} \text{ erg s}^{-1}$. This implies an accretion rate (in Eddington units) of $L_{\text{disk}}/L_{\text{Edd}} = 0.006$. Such a low-accretion rate suggests a radiatively inefficient accretion process and is expected in extreme blazars.

4.2. General theoretical considerations

The following section considers general energetics requirements for the production of a detectable IceCube neutrino flux in the jet of BZB J0955+3551. These considerations are constrained by the observed UV – X-ray flux just after the detection of the neutrino event, on January 8, 2020 and are similar to general energetics constraints on neutrino production in TXS 0506+056 by Reimer et al. (2019). Specifically a flux around $\sim 10^{16} - 10^{17} \text{ Hz}$ of $\nu F_{\nu}^{\text{UV-X}} \sim 10^{-12} F_{\text{UV},-12} \text{ erg cm}^{-2} \text{ s}^{-1}$ was observed, while the peak of the (presumably synchrotron) X-ray spectrum was located around $\sim 10^{18} \text{ Hz}$ at a flux close to $\nu F_{\nu} \sim 10^{-11} F_{\text{X},-11} \text{ erg cm}^{-2} \text{ s}^{-1}$ (Figure 3, left panel). We first derive a general constraint on the jet content of protons that might potentially be responsible for very high-energy (VHE) neutrino production, and then consider two possibilities for the source of target photons for photo-pion production on those protons.

We assume that neutrinos are produced in the same compact ($R \sim 10^{16} R_{16} \text{ cm}$) emission region as the high-energy (X-ray through γ -ray) electromagnetic radiation from the blazar. This emission region propagates along the jet with Lorentz factor $\Gamma = 10 \Gamma_1$, leading to Doppler boosting characterized by a Doppler factor $D = 10 D_1$. In the following, primes denote quantities in the rest-frame of this emission region. The redshift of $z = 0.5573$ corresponds to a luminosity distance of $d_L \sim 3.2 \text{ Gpc} \sim 9.7 \times 10^{27} \text{ cm}$.

4.3. Proton-photon interactions and neutrino production

In AGN jets, neutrinos are most plausibly produced through photo-hadronic interactions of relativistic protons of energy $E'_p = \gamma_p m_p c^2$ (in the rest-frame of the emission region) with target photons of (emission-region-frame) energy E'_t . This interaction is most

efficient when the center-of-momentum frame energy squared, $s = m_p c^2 + 2 E'_p E'_t (1 - \beta_p \cos \theta)$ — where $\beta_p = \sqrt{1 - 1/\gamma_p^2}$ is the normalized velocity (in units of the speed of light c) and γ_p the Lorentz factor of the proton — of the interaction is near the Δ^+ resonance, $s \sim E_{\Delta^+}^2 = (1232 \text{ MeV})^2$. This translates into a condition $E'_p E'_t \sim 3.2 \times 10^5 \text{ GeV}^2$.

The proton energy required to produce neutrinos at observed (i.e., Doppler-boosted) energies of hundreds of TeV, $E_{\nu} \equiv 100 E_{14} \text{ TeV}$ is $E'_p \simeq 200 E_{14}/(D_1 \xi_{0.05}) \text{ TeV}$ (i.e., $\gamma'_p = E'_p/m_p c^2 \simeq 2 \times 10^5 E_{14}/(D_1 \xi_{0.05})$) where $\xi \equiv 0.05 \xi_{0.05}$ is the average neutrino energy per initial proton energy in photo-hadronic interactions (Mücke et al. 1999). The Larmor radius of protons with such energy is $r_L \sim 6.7 \times 10^{10} (\gamma/[2 \times 10^5]) B_2^{-1} \text{ cm}$, where $B = 100 B_2 \text{ G}$ is the magnetic field. This indicates that they are expected to be well confined within the emission region and can plausibly be accelerated by standard mechanisms, such as Diffusive Shock Acceleration.

For photo-pion (and neutrino) production by protons of this energy at the Δ^+ resonance, target photons of $E'_t \geq 1.6 D_1 \xi_{0.05}/E_{14} \text{ keV}$ are required. In section 4.5, we will discuss two extreme options for the source of such target photons: (a) the co-moving electron synchrotron radiation field, and (b) an external radiation field that is isotropic in the AGN rest frame. First, however, we derive constraints on the number of relativistic protons that may be present in the jet.

4.4. Constraints on Jet Power

Protons of energy $E'_p = 200 E_{14}/(D_1 \xi_{0.05}) \text{ TeV}$ radiate proton synchrotron radiation at a characteristic frequency of

$$\begin{aligned} \nu_{\text{psy}}^{\text{obs}} &= 4.2 \times 10^6 B_G \gamma_p^2 D (m_e/m_p) \text{ Hz} \\ &\approx 9.2 \times 10^{16} \frac{B_2 E_{14}^2}{(D_1 \xi_{0.05}^2)} \text{ Hz}, \end{aligned} \quad (2)$$

i.e., in soft X-rays. Given a number of protons of energy γ_p , i.e., $N_p(\gamma_p) \sim \gamma_p dN_p(\gamma_p)/d\gamma_p$, one may calculate the produced co-moving luminosity in proton synchrotron radiation as

$$\begin{aligned} L'_{\text{psy}} &\approx \frac{c \sigma_T B^2}{6\pi} \left(\frac{m_e}{m_p} \right)^2 \gamma_p^3 \frac{dN_p(\gamma_p)}{d\gamma_p} \\ &\approx 2.5 \times 10^{-2} \frac{dN_p(\gamma_p)}{d\gamma_p} B_2^2 \frac{E_{14}^3}{D_1^3 \xi_{0.05}^3} \text{ erg s}^{-1}. \end{aligned} \quad (3)$$

The resulting observable soft X-ray flux, $\nu F_{\nu}^{\text{psy}} \sim D_1^2 L'_{\text{psy}}/(4\pi d_L^2)$ may not over-shoot the actually ob-

served UV – soft X-ray flux, thus constraining the differential number of protons to

$$\frac{dN_p(\gamma_p)}{d\gamma_p} \lesssim 4.7 \times 10^{42} \frac{F_{-12} \xi_{0.05}^3}{B_2^2 D_1 E_{14}^3}. \quad (4)$$

We consider a proton spectrum of the form $N_p(\gamma_p) = N_0 \gamma_p^{-\alpha_p}$ with $\alpha_p = 2$, extending from $\gamma_{p,\min} = 1$ to $\gamma_{p,\max} \sim 2 \times 10^5 E_{14}/(D_1 \xi_{0.05})$ so that the resulting proton synchrotron spectrum actually peaks (in νF_ν representation) at the characteristic proton synchrotron frequency ν_{psy} evaluated in Eq. (2) above. The proton-spectrum normalization is then constrained to

$$N_0 \lesssim 1.9 \times 10^{53} \frac{F_{-12} \xi_{0.05}}{B_2^2 D_1^3 E_{14}} \quad (5)$$

limiting the kinetic jet power in relativistic protons to

$$L_p \sim \frac{3 \Gamma^2 c (m_p c^2) N_0}{4 R} \ln \gamma_{p,\max} \lesssim 6.4 \times 10^{46} \frac{F_{-12} \xi_{0.05} \Gamma_1^2}{B_2^2 D_1^3 E_{14} R_{16}} (12.2 + \eta) \text{ erg s}^{-1}, \quad (6)$$

where $\eta \equiv \ln(E_{14}/[D_1 \xi_{0.05}])$. For $\eta = 0$ and all baseline parameters, Eq. (6) evaluates to $7.8 \times 10^{47} \text{ erg s}^{-1}$. In the following, we ignore the (presumed small) correction arising from potential values of $\eta \neq 0$.

Using the proton spectrum with normalization given by Eq. (5), we may estimate the co-moving neutrino luminosity through the proton energy loss rate due to photo-pion production, given by Kelner & Aharonian (2008)

$$\dot{\gamma}_{p,p\gamma} \approx -c \langle \sigma_{p\gamma} f \rangle n'_{\text{ph}}(\epsilon'_t) \epsilon'_t \gamma_p \quad (7)$$

where $\epsilon'_t = E'_t/(m_e c^2)$ and $\langle \sigma_{p\gamma} f \rangle \approx 10^{-28} \text{ cm}^2$ is the elasticity-weighted $p\gamma$ interaction cross section. The factor $n'_{\text{ph}}(\epsilon'_t) \epsilon'_t$ provides a proxy for the co-moving energy density of the target photon field, $u'_t \approx m_e c^2 n'_{\text{ph}}(\epsilon'_t) \epsilon'_t$. Considering that the energy lost by protons in $p\gamma$ interactions is shared approximately equally between photons and neutrinos, the VHE neutrino luminosity is given by

$$L'_\nu \approx \frac{1}{2} N_0 m_p c^2 \int_{\gamma_1}^{\gamma_{p,\max}} \gamma_p^{-2} |\dot{\gamma}_{p,p\gamma}| d\gamma_p \approx \frac{1}{2} c N_0 m_p c^2 \langle \sigma_{p\gamma} f \rangle \frac{u'_t}{m_e c^2} \ln \left(\frac{\gamma_{p,\max}}{\gamma_1} \right) \quad (8)$$

Considering that the target photon is unlikely to be mono-energetic, we set the lower limit in the integral in Eq. (8) to $\gamma_1 = 6.4 \times 10^4/(D_1 \xi_{0.05})$, corresponding to

protons producing neutrinos with an observed energy of $\sim 30 \text{ TeV}$. With this choice, the limit on the neutrino luminosity (corresponding to the limit on N_0 from Eq. 5) evaluates to

$$L'_\nu \lesssim 5.2 \times 10^{38} \frac{u'_t}{\text{erg cm}^{-3}} \ln(3.1 E_{14}) \frac{F_{-12} \xi_{0.05}}{B_2^2 D_1^3 E_{14}} \text{ erg s}^{-1}, \quad (9)$$

which yields a limit on the VHE neutrino flux measured on Earth as

$$F_\nu \lesssim 4.4 \times 10^{-15} \frac{u'_t}{\text{erg cm}^{-3}} \ln(3.1 E_{14}) \frac{F_{-12} \xi_{0.05} D_1}{B_2^2 E_{14}} \text{ erg cm}^{-2} \text{ s}^{-1}. \quad (10)$$

The single neutrino detection of IC-200107A corresponds to an approximate neutrino energy flux of $F_\nu^{\text{obs}} \sim 5 \times 10^{-11} F_{\nu,5e-11} \text{ erg cm}^{-2} \text{ s}^{-1}$, assuming a time window of one month and an E^{-2} spectrum and adopting the published effective area for the real-time stream (i.e., gold and bronze and HESE events; Blaufuss et al. 2019). We note that IC-200107A did not pass the current starting track classification but was identified by a new neural network classifier. The new classification is expected to provide an improved effective area for the HESE stream. However, since the HESE effective area is subdominant compared to the gold and bronze effective areas this will not significantly effect our estimated neutrino flux. Thus, Eq. (10) translates into a limit on the co-moving target photon field energy density of

$$u'_t \gtrsim 1.1 \times 10^4 \frac{B_2^2 E_{14} F_{\nu,5e-11}}{F_{-12} D_1 \xi_{0.05} \ln(3.1 E_{14})} \text{ erg cm}^{-3}. \quad (11)$$

Accounting for a possible Eddington bias due to the large number of potentially similar blazars from which no neutrinos have been detected (Strotjohann et al. 2019), the actual neutrino flux from this individual source may, however, be up to a factor of ~ 100 lower than the estimate provided above, i.e., $F_{\nu,5e-11} \gtrsim 10^{-2}$. In the following, we will discuss implications for the nature of such a target photon field.

4.5. Implications on the target photon fields

We will distinguish two possible scenarios, which can be thought of as extreme, limiting cases: (a) a target photon field that is co-moving with the emission region (such as the electron-synchrotron emission), or (b) a stationary target photon field in the AGN rest frame.

4.5.1. a) Co-moving target photon field

If the target photon field is co-moving (e.g., the electron-synchrotron photon field, which is routinely

used in lepto-hadronic blazar models as targets for photo-pion production), the target photon energy E'_t corresponds to an observed photon energy of $E_{t,\text{obs}} \geq 16 D_1^2 \xi_{0.05} / E_{14}$ keV (i.e., hard X-rays). The directly observed X-ray flux corresponding to the co-moving radiation energy density from Eq. (11) is, in this case, Doppler boosted by a factor of D^4 with respect to the observer, yielding a lower limit on the X-ray flux from this radiation field of

$$F_t^{\text{obs,a}} \sim \frac{D^4 R^2 c u'_t}{d_L^2} \gtrsim 3.5 \times 10^{-6} \frac{F_{\nu,5e-11} R_{16}^2 B_2^2 E_{14} D_1^3}{F_{-12} \xi_{0.05} \ln(3.1 E_{14})} \text{ erg cm}^{-2} \text{ s}^{-1}. \quad (12)$$

For any plausible choice of parameters, even with $F_{\nu,5e-11} \sim 10^{-2}$, this appears to be in clear violation of the observed X-ray flux of $\lesssim 10^{-11} \text{ erg cm}^{-2} \text{ s}^{-1}$. Just as in the case of TXS 0506+056 (see Reimer et al. 2019), we may therefore safely rule out the possibility of the co-moving electron synchrotron radiation field being the dominant target photon field for photo-pion production to produce a significant flux of VHE neutrinos.

4.5.2. b) Stationary photon field in the AGN rest frame

In the case of a photon field that is stationary (and quasi-isotropic) in the AGN rest frame, the external (stationary) target photon field is Doppler boosted into the blob frame, so that $E_{t,\text{obs}} \geq 0.16 \xi_{0.05} / E_{14}$ keV (i.e., UV-to-soft X-rays). In this case, the target photon density is enhanced in the co-moving frame, compared to the AGN-rest-frame energy density $u_t^{\text{AGN}} \sim u'_t / \Gamma^2$. Assuming that the target photon field originates in a larger region of size $R_t = 10^{17} R_{t,17}$ cm surrounding the jet, the resulting, directly observable UV – soft X-ray flux amounts to

$$F_t^{\text{obs,b}} \sim \frac{u'_t R_t^2 c}{\Gamma^2 d_L^2} \quad 3.5 \times 10^{-10} \frac{F_{\nu,5e-11} R_{t,17}^2 B_2^2 E_{14}}{D_1 \Gamma_1^2 F_{-12} \xi_{0.05} \ln(3.1 E_{14})} \text{ erg cm}^{-2} \text{ s}^{-1}. \quad (13)$$

Such a flux may well be compatible with the observed UV – soft X-ray flux of $\sim 10^{-12} \text{ erg cm}^{-2} \text{ s}^{-1}$, e.g., in case of a slightly smaller value of $R_t < 10^{17}$ cm or larger bulk Lorentz and Doppler factors, $\Gamma > 10$ and/or $D > 10$, especially if $F_{\nu,5e-11} \sim 10^{-2}$, i.e., the neutrino flux based on a single neutrino is indeed grossly overestimated due to the Eddington bias.

We therefore conclude that any plausible photo-hadronic neutrino production scenario in the jet of BZB J0955+3551 must involve a prominent external target radiation field.

In the following, we will therefore further investigate the possibility of photo-hadronic neutrino production in BZB J0955+3551 with an external target photon field, and check whether the observed optical – UV – X-ray spectrum is consistent with constraints from electromagnetic cascades initiated by the neutrino-producing pion and muon decay processes.

4.6. Numerical Simulations

Following the analytical considerations in the previous sub-sections, we now attempt to reproduce the observed neutrino flux with a detailed numerical model while not overshooting the observed emission. We employ the steady-state, single-zone lepto-hadronic model described in Böttcher et al. (2013), using parameters very close to the ones derived from the analytical estimates. The external photon field required for photo-hadronic neutrino production is represented by an equivalent electron-synchrotron radiation field with the same characteristics (i.e., co-moving energy density $u'_t = 1.14 \times 10^4 \text{ erg cm}^{-3}$ and peak frequency $\nu'_t = 3.5 \times 10^{17} \text{ Hz}$) because the code of Böttcher et al. (2013) does currently not include external radiation fields for photo-pion production. It has been shown (Böttcher et al. 2019) that the anisotropy of the target photon field has a negligible effect on the neutrino production and electromagnetic radiation output. Thus, our equivalent electron-synchrotron radiation set-up is an appropriate proxy for the required external target photon field. The results of the simulation are shown in Figure 3 with red and violet solid lines. The corresponding parameters are listed in Table 2. The very intense target photon field provides a very high $\gamma\gamma$ opacity for γ -rays in the *Fermi*-LAT energy range and higher, analogous to what was found for TXS 0506+056 (Reimer et al. 2019). This suggests that one would not expect a significant correlation between neutrino and γ -ray activity. The dashed model curves in Figure 3 show an attempt to reproduce the neutrino flux of $5 \times 10^{-11} \text{ erg cm}^{-2} \text{ s}^{-1}$, i.e., neglecting the Eddington bias. For this purpose, the proton power was increased by a factor of 100 with respect to the previous simulation, leaving all other parameters unchanged. It is obvious that, in this case, the electromagnetic output from proton synchrotron and cascades overshoots the X-ray fluxes and, even more so, the IR-optical-UV fluxes. This can, therefore, be ruled out. Overall, our results suggest a scenario in which a relativistic proton population responsible for the observed neutrino emission

Table 2. Parameters used/derived from the numerical simulation. The shape of the proton spectrum is adopted as a power law.

Parameter	Value
Co-moving photon field energy density (erg cm^{-3})	1.14×10^4
Co-moving photon field peak frequency (Hz)	3.5×10^{17}
Magnetic field (Gauss)	100
Bulk Lorentz factor	10
Emission-region radius (cm)	1×10^{16}
Viewing angle (degrees)	5.7
Low-energy cut-off of proton spectrum (GeV)	1
Proton high-energy cut-off (GeV)	10^6
Proton Injection spectral index	1.1
Kinetic luminosity in protons (erg s^{-1})	4×10^{46}
Magnetic jet power (erg s^{-1})	3.75×10^{47}

from BZB J0955+3551 may only make a sub-dominant contribution to the observed X-ray flare.

5. SUMMARY

We have followed the X-ray flaring activity of BZB J0955+3551 (Giommi et al. 2020b; Krauss et al. 2020) with *NuSTAR*, *Swift*, and GTC and also used the simultaneous observation from *NICER*. Using the high-quality OSIRIS spectrum, we determined the spectroscopic redshift of the blazar as $z = 0.5573$. On the other hand, we could not ascertain the nature of the companion object identified $\sim 3''$ South-East of BZB J0955+3551 in the i' filter Pan-STARRS image. Moreover, the optical spectrum of the source reveals a faint [O II]3727 emission line with rest-frame equivalent width of $0.15 \pm 0.05 \text{ \AA}$. We estimated a very low-level of accretion activity which is consistent with that expected from BL Lac objects. There are tentative evidences ($\lesssim 3.5\sigma$) for the hour-scale flux variability in the X-ray band, as estimated from the *NuSTAR* and *NICER* light curves. Finally, we showed that an external photon field is required to explain the neutrino emission and that a sub-dominant, i.e., not overshooting the observed optical-to-X-ray fluxes, hadronic population may be contributing to the expected neutrino flux.

REFERENCES

- Aartsen, M. G., Ackermann, M., Adams, J., et al. 2015, *ApJ*, 807, 46, doi: [10.1088/0004-637X/807/1/46](https://doi.org/10.1088/0004-637X/807/1/46)
- Aartsen, M. G., Abraham, K., Ackermann, M., et al. 2017, *ApJ*, 835, 151, doi: [10.3847/1538-4357/835/2/151](https://doi.org/10.3847/1538-4357/835/2/151)
- Aartsen, M. G., et al. 2020, *Phys. Rev. Lett.*, 124, 051103, doi: [10.1103/PhysRevLett.124.051103](https://doi.org/10.1103/PhysRevLett.124.051103)
- Arnaud, K. A. 1996, in *Astronomical Society of the Pacific Conference Series*, Vol. 101, *Astronomical Data Analysis Software and Systems V*, ed. G. H. Jacoby & J. Barnes, 17
- Blaufuss, E., Kintscher, T., Lu, L., & Tung, C. F. 2019, in *International Cosmic Ray Conference*, Vol. 36, 36th International Cosmic Ray Conference (ICRC2019), 1021. <https://arxiv.org/abs/1908.04884>
- Böttcher, M., Reimer, A., Buson, S., & Abdalla, H. 2019, in *TeV Particle Astrophysics (TeVPA 2019)*, *International Cosmic Ray Conference*, 3590902, doi: <https://indico.cern.ch/event/828038/contributions/3590902/>
- Böttcher, M., Reimer, A., Sweeney, K., & Prakash, A. 2013, *ApJ*, 768, 54, doi: [10.1088/0004-637X/768/1/54](https://doi.org/10.1088/0004-637X/768/1/54)
- Breeveld, A. A., Landsman, W., Holland, S. T., et al. 2011, in *American Institute of Physics Conference Series*, Vol. 1358, *American Institute of Physics Conference Series*, ed. J. E. McEnery, J. L. Racusin, & N. Gehrels, 373–376, doi: [10.1063/1.3621807](https://doi.org/10.1063/1.3621807)
- Cepa, J., Aguiar, M., Escalera, V. G., et al. 2000, in *Proc. SPIE*, Vol. 4008, *Optical and IR Telescope Instrumentation and Detectors*, ed. M. Iye & A. F. Moorwood, 623–631, doi: [10.1117/12.395520](https://doi.org/10.1117/12.395520)
- Cepa, J., Aguiar-Gonzalez, M., Bland-Hawthorn, J., et al. 2003, in *Proc. SPIE*, Vol. 4841, *Instrument Design and Performance for Optical/Infrared Ground-based Telescopes*, ed. M. Iye & A. F. M. Moorwood, 1739–1749, doi: [10.1117/12.460913](https://doi.org/10.1117/12.460913)
- Costamante, L., Bonnoli, G., Tavecchio, F., et al. 2018, *MNRAS*, 477, 4257, doi: [10.1093/mnras/sty857](https://doi.org/10.1093/mnras/sty857)
- Costamante, L., Ghisellini, G., Giommi, P., et al. 2001, *A&A*, 371, 512, doi: [10.1051/0004-6361:20010412](https://doi.org/10.1051/0004-6361:20010412)
- Domínguez, A., Primack, J. R., Rosario, D. J., et al. 2011, *MNRAS*, 410, 2556, doi: [10.1111/j.1365-2966.2010.17631.x](https://doi.org/10.1111/j.1365-2966.2010.17631.x)
- Foffano, L., Prandini, E., Franceschini, A., & Paiano, S. 2019, *MNRAS*, 486, 1741, doi: [10.1093/mnras/stz812](https://doi.org/10.1093/mnras/stz812)
- Garrappa, S., Buson, S., & Fermi-LAT Collaboration. 2020, *GRB Coordinates Network*, 26669, 1
- Garrappa, S., Buson, S., Franckowiak, A., et al. 2019, *The Astrophysical Journal*, 880, 103, doi: [10.3847/1538-4357/ab2ada](https://doi.org/10.3847/1538-4357/ab2ada)

- Giommi, P., Glauch, T., Padovani, P., et al. 2020a, arXiv e-prints, arXiv:2001.09355.
<https://arxiv.org/abs/2001.09355>
- Giommi, P., Glauch, T., & Resconi, E. 2020b, The Astronomer’s Telegram, 13394, 1
- Giommi, P., Polenta, G., Lähtenmäki, A., et al. 2012, A&A, 541, A160, doi: [10.1051/0004-6361/201117825](https://doi.org/10.1051/0004-6361/201117825)
- IceCube Collaboration. 2020, GRB Coordinates Network, 26655, 1
- IceCube Collaboration, Aartsen, M. G., Ackermann, M., et al. 2018a, Science, 361, eaat1378, doi: [10.1126/science.aat1378](https://doi.org/10.1126/science.aat1378)
- . 2018b, Science, 361, 147, doi: [10.1126/science.aat2890](https://doi.org/10.1126/science.aat2890)
- Kalberla, P. M. W., Burton, W. B., Hartmann, D., et al. 2005, A&A, 440, 775, doi: [10.1051/0004-6361:20041864](https://doi.org/10.1051/0004-6361:20041864)
- Kelner, S. R., & Aharonian, F. A. 2008, PhRvD, 78, 034013, doi: [10.1103/PhysRevD.78.034013](https://doi.org/10.1103/PhysRevD.78.034013)
- King, D. L. 1985, ING Technical Note, 31, https://www.ing.iac.es/Astronomy/observing/manuals/ps/tech_notes/tn031.pdf
- Krauss, F., Gregoire, T., Fox, D. B., Kennea, J., & Evans, P. 2020, The Astronomer’s Telegram, 13395, 1
- Lucarelli, F., Tavani, M., Piano, G., et al. 2019, ApJ, 870, 136, doi: [10.3847/1538-4357/aaf1c0](https://doi.org/10.3847/1538-4357/aaf1c0)
- Mannheim, K., Staney, T., & Biermann, P. L. 1992, A&A, 260, L1
- McLure, R. J., & Dunlop, J. S. 2002, MNRAS, 331, 795, doi: [10.1046/j.1365-8711.2002.05236.x](https://doi.org/10.1046/j.1365-8711.2002.05236.x)
- Mücke, A., Rachen, J. P., Engel, R., Protheroe, R. J., & Staney, T. 1999, PASA, 16, 160, doi: [10.1071/AS99160](https://doi.org/10.1071/AS99160)
- Murase, K. 2017, Active Galactic Nuclei as High-Energy Neutrino Sources, ed. T. Gaisser & A. Karle, 15–31, doi: [10.1142/9789814759410_0002](https://doi.org/10.1142/9789814759410_0002)
- Padovani, P., Oikonomou, F., Petropoulou, M., Giommi, P., & Resconi, E. 2019, MNRAS, 484, L104, doi: [10.1093/mnrasl/slz011](https://doi.org/10.1093/mnrasl/slz011)
- Padovani, P., Resconi, E., Giommi, P., Arsioli, B., & Chang, Y. L. 2016, MNRAS, 457, 3582, doi: [10.1093/mnras/stw228](https://doi.org/10.1093/mnras/stw228)
- Paliya, V. S., Domínguez, A., Ajello, M., Franckowiak, A., & Hartmann, D. 2019, ApJL, 882, L3, doi: [10.3847/2041-8213/ab398a](https://doi.org/10.3847/2041-8213/ab398a)
- Petropoulou, M., Dimitrakoudis, S., Padovani, P., Mastichiadis, A., & Resconi, E. 2015, MNRAS, 448, 2412, doi: [10.1093/mnras/stv179](https://doi.org/10.1093/mnras/stv179)
- Planck Collaboration, Ade, P. A. R., Aghanim, N., et al. 2016, A&A, 594, A13, doi: [10.1051/0004-6361/201525830](https://doi.org/10.1051/0004-6361/201525830)
- Punsly, B., & Zhang, S. 2011, MNRAS, 412, L123, doi: [10.1111/j.1745-3933.2011.01019.x](https://doi.org/10.1111/j.1745-3933.2011.01019.x)
- Reimer, A., Böttcher, M., & Buson, S. 2019, ApJ, 881, 46, doi: [10.3847/1538-4357/ab2bff](https://doi.org/10.3847/1538-4357/ab2bff)
- Richards, G. T., Lacy, M., Storrie-Lombardi, L. J., et al. 2006, ApJS, 166, 470, doi: [10.1086/506525](https://doi.org/10.1086/506525)
- Schlaflly, E. F., & Finkbeiner, D. P. 2011, ApJ, 737, 103, doi: [10.1088/0004-637X/737/2/103](https://doi.org/10.1088/0004-637X/737/2/103)
- Stickel, M., Padovani, P., Urry, C. M., Fried, J. W., & Kuehr, H. 1991, ApJ, 374, 431, doi: [10.1086/170133](https://doi.org/10.1086/170133)
- Strotjohann, N. L., Kowalski, M., & Franckowiak, A. 2019, A&A, 622, L9, doi: [10.1051/0004-6361/201834750](https://doi.org/10.1051/0004-6361/201834750)
- The Fermi-LAT collaboration. 2019, arXiv e-prints, arXiv:1902.10045. <https://arxiv.org/abs/1902.10045>
- van Dokkum, P. G. 2001, PASP, 113, 1420, doi: [10.1086/323894](https://doi.org/10.1086/323894)

ACKNOWLEDGMENTS

This work was supported by the Initiative and Networking Fund of the Helmholtz Association. We are thankful to *NuSTAR*, and *Swift* PIs for approving our DDT requests and to the mission operations team for quickly scheduling the observations. Thanks are also due to *NICER* PI for observing the source as a DDT ToO. A.D. acknowledges the support of the Ramón y Cajal program from the Spanish MINECO. We are grateful to staff astronomers Antonio Cabrera at GTC for carrying out OSIRIS observation. This work is based on observations made with the GTC telescope, in the Spanish Observatorio del Roque de los Muchachos of the Instituto de Astrofísica de Canarias, under Directors Discretionary Time. The work of M.B. is supported through the South African Research Chair Initiative of the National Research Foundation⁵ and the Department of Science and Innovation of South Africa, under SARChI Chair grant No. 64789. A.G.P. and A.O.G. acknowledge financial support from the Spanish Ministry of Economy and Competitiveness (MINECO) under grant numbers AYA2016-75808-R and RTI2018-096188-B-I00, which are partly funded by the European Regional Development Fund (ERDF). A.O.G. also acknowledges financial support from the Comunidad de Madrid Tec2Space project S2018/NMT-4291.

Facilities: S